6

Impact of excess Sn and low temperature processing on Cu_2ZnSnS_4 and their device performance: A ^{119}Sn Mossbauer Study

6.1 Introduction

Kesterite material Cu_2ZnSnS_4, also named as CZTS, has emerged as a promising photovoltaic (PV) absorber layer material. Its attractive optical and electronic properties such as high absorption coefficient and optimum direct band gap make it a suitable alternative for silicon photovoltaics. In addition, this is considered as a good replacement for existing chalcopyrite $CuInGaSe_2$ (CIGS) absorber, which already demonstrated a large photovoltaic efficiency of about 22.6% [Jackson et al., 2016]. Kesterites bear the advantages of their low cost earth abundant constituents, unlike chalcopyrite which suffers with indium scarcity and gallium (Ga) toxicity. Further, the bandgap tunability by alloying with selenium favours the optimization of bandgap to match the solar spectrum realizing the enhanced photoconversion efficiency. Several vacuum and non-vacuum based deposition methods are optimized till date to fabricate CZTSSe based solar photovoltaic devices with significant efficiencies [Shin, Zhu, Bojarczuk, Jay Chey, & Guha, 2012b][Tao et al., 2016][Cao et al., 2012][Larramona et al., 2015][T. K. Todorov et al., 2013]. However, the maximum efficiency is still far behind the Schockley-Quieser limit (~ 32.8%) for CZTS,Se solar cell [Siebentritt, 2013]. The pure sulfide CZTS and selenide CZTSe based photovoltaic devices reached the maximum efficiency upto 9.2% and 11.6%, synthesized with co-evaporation techniques [Takuya Kato, Homare Hiroi, Noriyuki Sakai, Satoshi Muraoka, 2012][Lee et al., 2015]. Further, sulfoselenide CZTSSe absorber based photovoltaic cell showed the maximum efficiency ~ 12.6% and ~ 12.7% with single CdS buffer layer and with double CdS/In_2S_3 buffer layer using hydrazine based pure solution approach[W. Wang et al., 2014][Jeehwan Kim et al., 2014]. Kesterite solar devices commonly suffers from the problem of voltage deficit which presents a significant challenge in realizing the high efficiency [Hages, Carter, Agrawal, & Unold, 2014][Crovetto et al., 2017]. Recently Priscilla D. Antunez et al.[Antunez, Bishop, Luo, & Haight, 2017] has reported near the maximum efficiency ~ 10.6%, reported with high open circuit voltage, by exfoliation of back contact from the growth substrate and then depositing the high work function back contact on the grown device. Incorporation of Ge in CZTS,Se also shows significant possibility to get rid of voltage deficit problem [Shinho Kim et al., 2016]. There are numerous materials and device issues and challenges to realize high photovoltaic efficiencies with CZTS. Further, being a quaternary material this system is prone to acceptor and donor type defects and has a very narrow region of phase stability. Defects in the CZTS system includes vacancies (V_{Cu}, V_{Zn}, V_{Sn}, V_S), antisites (Cu_{Zn}, Cu_{Sn}, Zn_{Sn}, $Zn_{Cu,}$ Sn_{Cu}, Sn_{Zn}) and interstitials (Cu_i, Zn_i, Sn_i, S_i) [S. Chen, Yang, et al., 2010]. Relatively lower formation energy of acceptor defects as compared to that of donor defects makes CZTS a p type material without any foreign element doping. Stoichiometric CZTS thin film shows inferior performance as compared to that of the non-stoichiometric films in terms of photovoltaic response [Delbos, 2012]. However non-stoichiometry sometimes may lead to the high density of defects and secondary phases, simultaneously, causing degraded performance [T. J. Huang et al., 2014][Mutter & Dunham, 2015].

Zn and Cu disorders are quite common because of similar chemical structures of Zn and Cu, such as ionic radii and nearly similar electronic configuration. These two atoms can easily swap at lower enthalpic cost to form Cu_{Zn} acceptor and Zn_{Cu} donor antisite defects [Bourdais et al., 2016][S. Chen, Gong, Walsh, & Wei, 2010]. Vacancy of Cu also introduces acceptor level. This vacancy at Cu site V_{Cu} and copper at zinc site Cu_{Zn} are dominant acceptor defects in CZTS system. These defects in conjunction [Cu_{Zn} + Zn_{Cu}] and [V_{Cu} +Zn_{Cu}] form defect complexes, which are self-compensating and with comparatively lower formation energy of Cu_{Zn} and V_{Cu} acceptor defects [Polizzotti, Repins, Noufi, Wei, & Mitzi, 2013]. These defects make CZTS a p-type semiconductor. Cu_{Zn} acceptor level is deep inside the band gap as compared to V_{Cu}. This suggests that acceptor carrier concentration in CZTS due to Cu_{Zn} is not the dominant source. It is also observed that even in stoichiometric CZTS, Cu_{Zn} + Sn_{Zn} and $2Cu_{Zn}$ + Sn_{Zn} defect clusters exhibit high concentration causing significant bandgap decrease and are detrimental to the device performance [S. Chen et al., 2016]. Therefore, Cu deficient and Zn rich configuration is suggested to be favorable for the high performing devices [Hironori Katagiri, Jimbo, Tahara, Araki, & Oishi, 2009][S. Chen, Gong, et al., 2010]. However, any non-stochiometry in CZTS allows the formation of unwanted binary and ternary impurity phases. Cu and Sn rich CZTS favors formation of Cu_2S, SnS, and Cu_2SnS_3 binary and ternary impurity compounds. These impurities are conductive and provide shunting paths in the device, thus decreasing the open circuit voltage. Zn rich CZTS favors the formation of ZnS impurity which is detrimental but passivate the probable shunt path present in the CZTS. Sn in CZTS lattice exits in +IV sate at its native site. However, Sn in CZTS can replace Cu and Zn from their lattice sites and can create antisite point defects Sn_{Cu} and Sn_{Zn}, deep in the bandgap and their high formation energy make them relatively uninfluential [S. Chen et al., 2016]. Further, multivalent Sn can exist in +II or +IV oxidation states. Sn at Cu site Sn_{Cu} exists exclusively as a divalent atom and forms shallow single donor level [Biswas, Lany, & Zunger, 2010] and Sn at the Zn site either forms double donor or isoelectronic center related to its multivalent nature. Isoelectronic centers, formed due to change in valancy of Sn from IV to II state, acts as non-radiative recombination centers, while at its +IV valance state, it forms deep donor level far from the conduction band and hence serves as the recombination center and not as a shallow donor. These defects in CZTS severely affect the photovoltaic response and hence should be avoided by taking care of nonstochiometry in CZTS [Biswas et al., 2010].

This chapter focuses on the effect of post annealing treatment on structural, optical, and electronic properties of sol-gel derived CZTS thin films. Mössbauer spectroscopic measurements are carried out to understand the local states of Sn ions in CZTS system and their impact on photovoltaic response. Temperature dependent resistance measurements are used to understand the activation energy of defects in CZTS samples. The prepared CZTS thin films are further integrated in Al:ZnO/iZnO/CdS/CZTS/Mo/Glass solar photovoltaic device structures. The fabricated devices are characterized for electrical and impedance properties to understand the photovoltaic response against process parameters.

6.2 Experimental details

CZTS thin films are prepared using sol-gel spin coating technique on 1″ x 1″ soda lime glass (SLG) substrates. These SLG substrates are ultrasonically cleaned as discussed earlier in **section 3.1**. Sol-gel derived spin coating process is used for non-vacuum CZTS thin film deposition. The solution for the spin coating is prepared in 2- methoxyethanol solvent using chloride salts of constituent metals and thiourea as the sulfur source, as discussed earlier in **section 4.2** [G. K. Gupta & Dixit, 2017]. The prepared highly stable sol is spin coated at around 3500 rpm followed by baking at 300 °C over hot plate in open ambient for 5 min. This spinning and drying process is repeated several time to get the desired thickness. The CZTS sample thus prepared is later kept at 300 °C in open atmosphere for 30 min and named as S1 for later discussion. An identical sample is annealed at 550 °C under 5% H_2S + Ar dynamic gaseous environment in a tubular single zone furnace as discussed in **section 5.2** to avoid any sulfur loss

from the system. The heating profile is reported earlier [G. K. Gupta, Garg, & Dixit, 2018]. The sample thus annealed is named as sample S2 for future discussion.

6.3 Result and Discussion

The measured XRD diffractographs are shown in **Figure 6.1** and the observed diffracted lines are indexed with kesterite CZTS phase (ICDD # 26-0575). The films are textured along (112) planar orientation and the crystallinity improves for high temperature treated sample S2. The improved intensity and reduced full width at half maxima (FWHM) of diffraction peaks for S2 CZTS sample, suggest the enhancement in the crystallinity with increased grain size. These measurements imply that annealing in H_2S environment at elevated temperature provides enough thermal energy to crystallize CZTS into larger grains in conjunction with supplementing any sulfur loss. The estimated average crystallite sizes using Scherrer formula are 77 Å, and 143 Å for samples S1, and S2, respectively. This controlled thermal treatment also assisted in reducing the dislocation density, which is calculated from the estimated average crystallite size by applying Williamson and Smallman equation $\delta=1/D^2$, where D is the average crystallite size [Williamson & Smallman, 1956]. The calculated dislocation densities are 1.68×10^{16} lines/m^2 and 4.89×10^{15} lines/m^2 for sample S1 and S2, respectively.

.

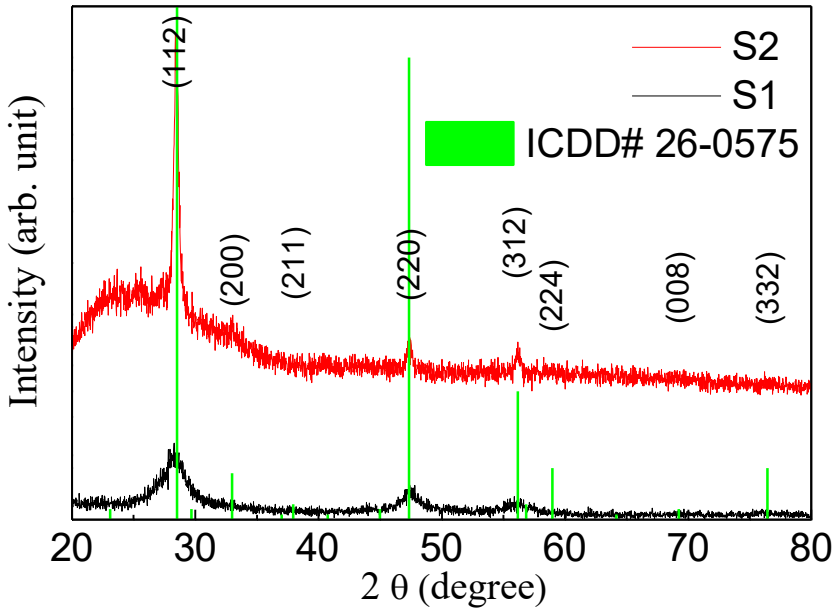

Figure 6.1 XRD patterns for sample S1, S2 (Green color lines indicate the peak positions of CZTS according to ICDD # 26-0575).

The microscopic and topographic measurements are summarized in **Figure 6.2** and suggest that films are smooth, dense and have large grains. The solution processed S1 and S2 samples are nearly free from any cracks and voids, **Figure 6.2 (a, c)**. EDAX results are summarized in **Table 6.1** for different elements in different CZTS samples. The elemental composition of these samples suggest copper poor and slightly tin rich configuration for S1 sample. Annealing at elevated temperature resulted in the loss of tin from the samples and is relatively poor in tin composition. The stoichiometry changes after post annealing treatment due to tin loss and sample S2 shows copper poor and zinc rich configuration. Both samples S1 and S2 are showing slightly excess sulfur content from stoichiometric ratio, however, the numbers are within the error limits of EDX measurements.

Table 6.1 Elemental composition for S1 and S2 samples, as extracted from EDX measurements, in conjunction with different atomic ratios

Samples	Cu	Zn	Sn	S	Cu/Zn+Sn	Zn/Sn	Cu/Sn	Cu/Zn
S1	21.72	12.51	13.41	52.36	0.838	0.93	1.62	1.74
S2	22.06	12.56	11.87	53.50	0.903	1.06	1.86	1.76

The controlled copper deficiency is important to realize the p-type electrical conductivity of CZTS material, an important parameter for designing high efficiency solar photovoltaic devices. The surface morphology shown in **Figure 6.2 (a)**, of S1 suggest dense but smaller grains which after annealing increases in S2 **Figure 6.2 (c)**. This is also in agreement with the observed improved crystallinity of sample S2 as compared to that of S1 in XRD micrograph. Topographic images of the prepared samples S1 and S2 are obtained using atomic force microscopy (AFM) and are shown in **Figure 6.2 (b, d)**. The roughness of the samples remains relatively immune with the annealing treatment. The observed RMS roughness, average roughness and grain length summarized in **Table 6.2**.

Table 6.2 Average, RMS roughness and grain size for S1 and S2 samples

Samples	Rq (nm)	Ra (nm)	Grain (nm)
S1	53.138	41.96	244.3
S2	50.1	40.5	344

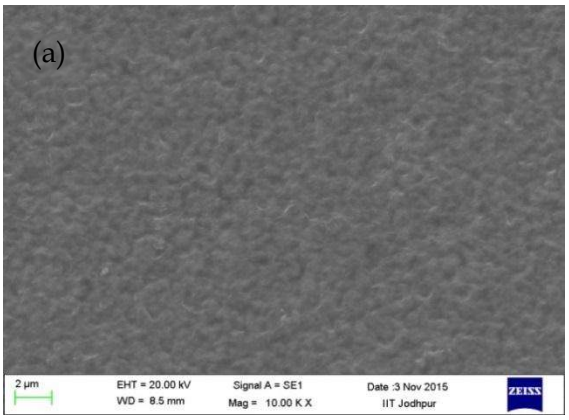

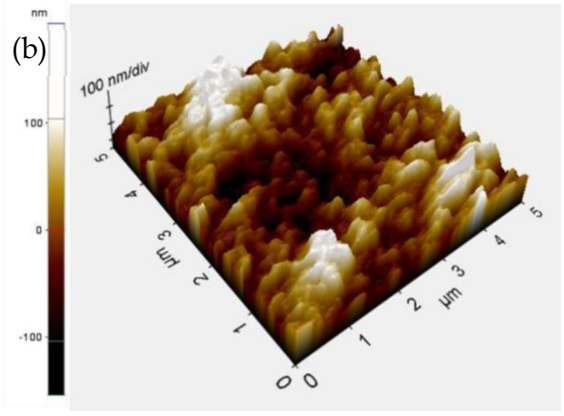

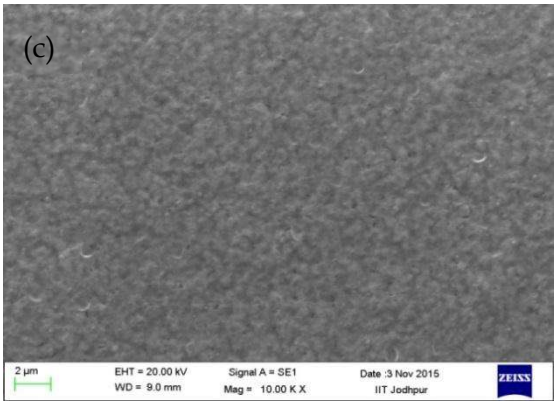

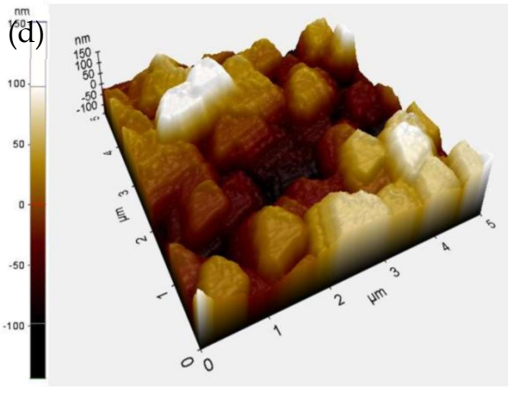

Figure 6.2 SEM micrograph for (a) S1 and (b) S2 surfaces; and respective topographic images (c) S1 and (d) S2 samples

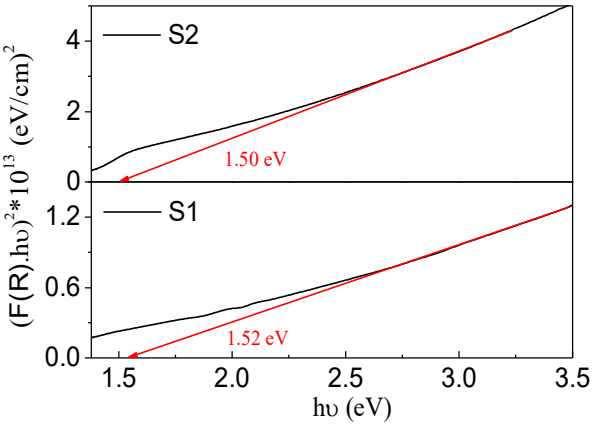

Figure 6.3 Tauc plot for CZTS thin film samples S1 and S2; used for estimating the band gap values

The optical properties are investigated using UV-Vis reflectance data for these samples. The measured reflectance is used to calculate the spectral absorbance F(R) using Kubelka-Munk model, $F(R) = {(100-R)^2}/{2R}$ and finally $(F(R).h\upsilon)^2$ as function of energy (hυ) is plotted in **Figure 6.3** for S1 and S2 samples. The absorption edge is evaluated from the extrapolated linear region of Tauc plot using $(F(R)h\nu)^2 = A(h\nu - E_g)$ relation, where Eg is the optical band gap of the material. The measured band gap values are close to 1.5 eV for both CZTS samples (S1 and S2), as explained using red arrow lines in **Figure 6.3**.

6.4 Mössbauer spectroscopic measurements

^{119}Sn Mössbauer spectroscopy measurements are carried out in transmission geometry for both pristine S1 and post annealed S2 CZTS thin films and the results are summarized in **Figure 6.4**

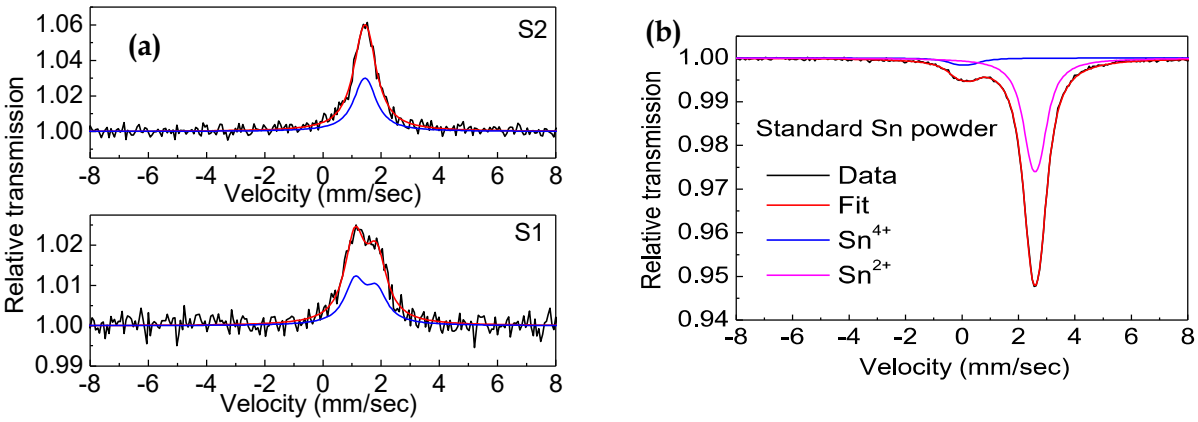

Figure 6.4 *^{119}Sn Mossbauer spectroscopic measurements on S1 and S2(a) CZTS samples, with standard Sn powder (b) as a reference.*

The data is fitted with a doublet for both S1 and S2 CZTS samples. The measured hyperfine parameters are shown in **Table 6.3**. In stoichiometric CZTS, oxidation states of Cu, Zn, Sn and S

are +I, +II, +IV, and –II, respectively. However, due to multivalancy of Sn it can exist in both +II and +IV oxidation states. One can get this information unambiguously from the obtained isomer shift values.

Mössbauer spectroscopy also probes the local environment around a nucleus and is very sensitive to local atomic structure affected by grain boundaries and the defects such as dislocations, antisites, vacancies and interstitials. The isomer shift (IS) obtained from the Mössbauer spectra is almost same for both the samples. With respect to SnO_2, the isomer shift (IS) values of about 2.5 mm/s or more are considered to be due to Sn^{2+} ions and tin (IV) compounds are expected to give IS values less than 2.0 mm/s [Banwell, 1983]. The observed IS values of both S1 and S2 sample indicate the presence of tetrahedral coordinated Sn^{4+} matching the result of Benedetto et al., in similar compounds [Di Benedetto et al., 2005]. However, there is considerable change in the quadruple splitting values for both the samples suggesting the different degree of distortion at Sn site with annealing. No isomer shift is observed for Sn^{2+}, thereby reducing the possibility of presence of Sn at Cu site forming Sn_{Cu} defect. The observed large quadruple splitting in S1 is possibly associated with the tetrahedral distortion/amorphization of Sn^{4+} ions, distributed randomly in the host CZTS matrix. The high atomic fraction of Sn observed in the S1 by EDX measurement also facilitates possibility of Sn to reside at the interstitial. The QS value decreases for high temperature annealed S2 sample. The relative lowering in QS value suggests that annealing resulted in more crystallization and thus reduced disorder of Sn^{4+} in CZTS system. The absence of Sn in +II valance state in the both the samples S1 and S2 is also governed by the presence of excess sulfur in the system, which restrict reduction of Sn^{4+} into Sn^{2+} to neutral charge states [Sunghyun Kim, Park, & Walsh, 2018].

Table 6.3 Isomer and Quadrupole shifts with FWHM and tin valance state parameters derived from ^{119}Sn Mossbauer data

Sample	IS (mm/s)	Q.S(mm/s)	FWHM (mm/s)	A21	Area (%)	State
S2	1.45 ± 0.01	0.19 ± 0.08	0.86 ± 0.05	1.00 (Fixed)	100	Sn^{2+}
S1	1.47 ± 0.02	0.74 ± 0.02	0.85 ± 0.04	1.33 ± 0.11	100	Sn^{4+}
Standard	0.01 ± 0.01	0.48 ± 0.04	0.93 ± 0.06	1.00	8.8	Sn^{4+}
	2.59 ± 0.01	0.29 ± 0.01	0.79 ± 0.01	1.00	92.2	Sn^{2+}

6.5 Electrical characterization

Temperature dependent electrical measurements are carried out from 100 K to 293 K temperature range using a liquid nitrogen cooled cryostat chamber. We normalized the measured two probe resistance and are shown in **Figure 6.5** for samples S1 and S2. The observed decreasing trend with increasing temperature confirms the semiconducting behavior of these CZTS thin films. The measured relative lower resistance for sample S2 is in agreement with the observed improved crystallinity of S2 sample, as discussed earlier. The improved crystallinity reduces the grain boundary barriers as compared to that of not annealed CZTS thin films (S1 sample).

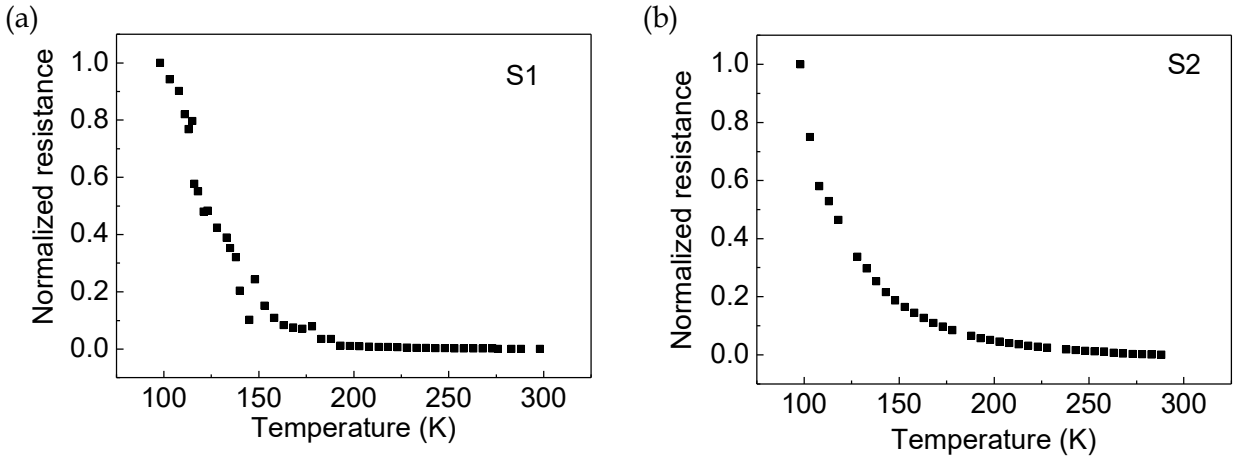

Figure 6.5 Normalized temperature dependent resistance variation with temperature for (a) S1 and (b) S2 CZTS samples

To understand closely the transport mechanism, natural logarithm of normalized conductance is plotted with respect to inverse of temperature (ln σ vs. 1000/T) from the normalized resistivity vs. temperature data and is shown in **Figure 6.6**. We observed that ln σ vs. 1000/T curves for S1 and S2 are comprised of two linear regions. At high temperature region for T> 250K the conduction in the film is governed by the thermionic emission and can be expressed as [B. L. Guo, Chen, Liu, Liu, & Li, 2014]

$$\sigma = \sigma_0 exp(-E_a/KT)$$

Where σ_0 is a pre-exponential factor proportional to the grain size and average carrier concentration present in the film, E_a is activation energy related to the barrier height in grain boundaries and '*K*' is Boltzman constant.

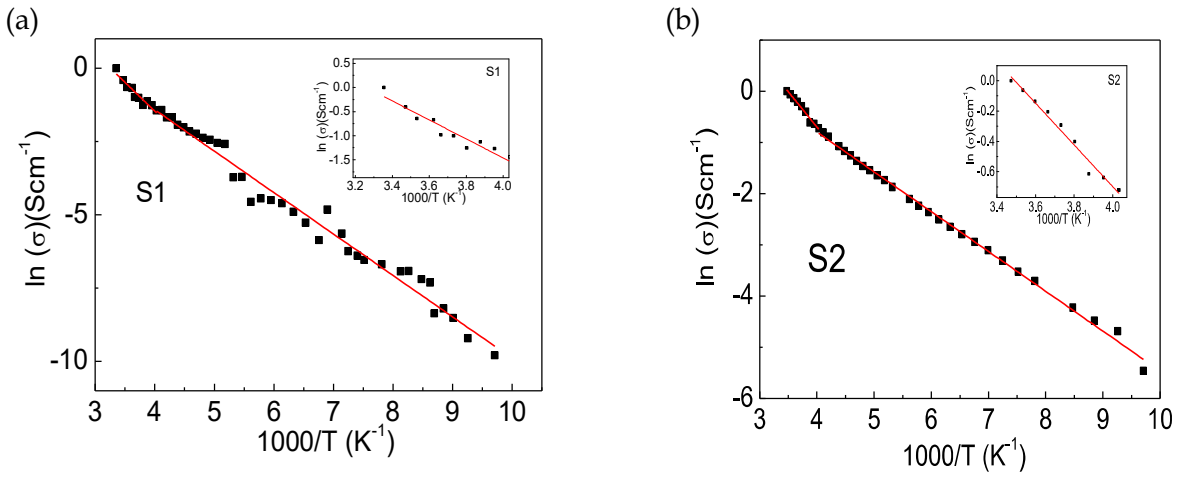

Figure 6.6 Natural logarithm of conductivity against 1000/T plots for (a) S1 and (b) S2 CZTS samples, with inset showing the high temperature regions for respective samples

Table 6.4 Activation energies for thermally activated and NNH carriers, as estimated from temperature dependent resistivity measurements.

Sample	Slope1	Slope2	E_a (meV)	E_{NNH} (meV)
S1	1.971	1.413	169.9	121.8
S2	1.376	0.777	118.7	67

The activation energy of ~ 169.9 meV and 118.7 meV are measured for S1 and S2 samples from the respective slopes of these ln σ vs. 1000/T curves in higher temperature region. At lower temperature, holes in the p type semiconductor do not have sufficient energy to jump from acceptor level to the valance band and the conduction is dominated by the hopping of charge carriers. For low temperature of ln σ vs. 1000/T curve is fitted with a straight line considering Nearest Neighbour Hopping (NNH) conduction mechanism. For NNH conduction in p type semiconductor hopping conductivity can be written as

$$\sigma = \sigma_{0NNH} exp(-E_{NNH}/KT)$$

Where σ_{0NNH} is a pre-exponential factor, E_{NNH} is activation energy for hopping conduction and *K* is Boltzmann constant. The estimated activation energy for NNH conduction is 121.8 meV and 67 meV for S1 and S2 CZTS thin films, respectively. These values are summarized in **Table 6.4**

.

6.6 Al:ZnO/i-ZnO/CdS/CZTS/Mo/SLG Device fabrication and characterization

A complete solar cell device structure Al:ZnO/i-ZnO/CdS/CZTS/Mo/SLG is fabricated with low temperature processed (S1) and high temperature treated (S2) CZTS samples. The fabrication of complete device is reported elsewhere [G. K. Gupta et al., 2018]. In brief, a 2.5 μm thick CZTS absorber layer is deposited over Mo coated SLG substrate, followed by a ~50 nm CdS thin layer deposition using chemical bath deposition. This CdS layer acts as the buffer layer and forms a p-n heterostructure junction with CZTS absorber layer. Thin intrinsic ZnO layer (~80 nm) is deposited using RF sputtering, as a window layer, which also protects the bottom layer during the DC sputter deposition of aluminum doped ZnO layer working as the transparent top contact.

6.7 Capacitance voltage characterization

Capacitance-voltage (C-V) characteristics are measured under different bias potentials at 5 kHz in dark for both low temperature (S1) and high temperature (S2) processed absorbers based photovoltaic devices. A relatively high frequency is considered intentionally to avoid the contribution of traps in the absorber layer in C-V measurements. The measured capacitance-voltage curves are shown in **Figure 6.7 (a)** for both the cells. The cell capacitance is dominated by the depletion or space charge capacitance at negative bias potential, whereas diffusion capacitance becomes significant with forward bias and an exponential increase in capacitance is observed with increasing voltage. The photovoltaic devices based on S1 and S2 absorbers exhibit different forward bias potentials for the exponential increase in capacitance values. This forward bias potential is relatively higher for S1 based absorber, suggesting that a higher potential is required for not annealed CZTS absorber based devices. This is attributed to the relatively lower carrier concentration in low temperature processed CZTS (S1 sample) as compared to that of high temperature processed CZTS (S2 sample) absorbers. Further, Mott-Schottkey plots (i.e plot of reciprocal of squared capacitance at different bias potential) are shown in **Figure 6.7 (b).**The observed negative Mott-Schottky slopes substantiate p- type conductivity of these CZTS films (both S1 and S2 CZTS thin films). This Mott-Schottky slope is used to calculate the carrier concentrations and values are 6.95 x10^{16} cm^{-3} and 2.51 x 10^{17} cm^{-3} for S1 and S2 CZTS thin film absorbers, respectively. Thus, observed relatively lower carrier concentration for S1 sample is in agreement with the observation that a large forward bias potential is required to drive the device into the diffusion capacitance region, **Figure 6.7 (a)**.

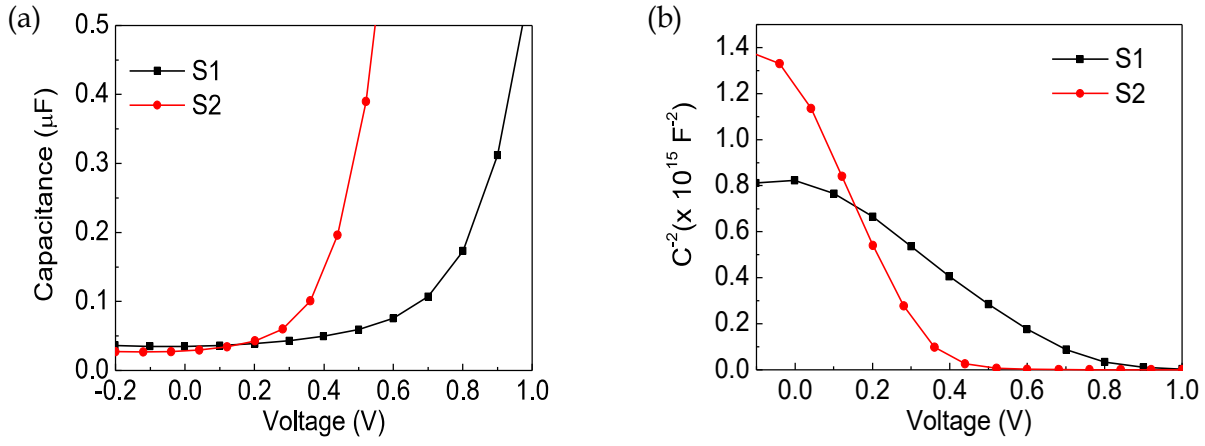

Figure 6.7 (a) Capacitance-Voltage (C-V) measurements (b) Mott-Schottky plots of photovoltaic devices based on S1 and S2 absorbers

The observed large carrier concentration for S2 as compared to S1 can be explained by the fact that tin based antisite defects acts as donor defects and serve to compensate the available most probable acceptor defects such as Cu_{Zn} and V_{Cu} present in the system. Since no signature of tin

at its +II valance state is observed in Mössbauer spectra hence possibility of Sn at Cu sites is not probable however there is high probability of presence of Sn at Zn site because of lower formation energy of Sn_{Zn}^{2+} in CZTS[S. Chen et al., 2013]. The increased conductivity of S2 is also in agreement with the theoretical reports suggesting that conductivity increases with increase in Cu/Sn ratio in the CZTS samples[Garcia-Hemme, Fairbrother, Calvo-Barrio, Saucedo, & Martil, 2016].

6.8 Photovoltaic characteristics

The photovoltaic performance of solar cells is taken under dark and under one Sun illumination for both S1 and S2 absorbers and is shown in **Figure 6.8**. The extracted device parameters are listed in **Table 6.5**.These observations suggest the improvement in efficiency for solar cell fabricated using S2 absorber. The obtained maximum efficiency values are 0.145% and 1.0% for S1 and S2 CZTS absorber based solar cells, respectively. The dark current densities are fitted with single diode model to obtain the reverse saturation current density (J_0) and the ideality factor (n) for these solar cell devices. The details are discussed in **section 5.3.3**. The measured (n, J_0) values are (4.32, 23.85 μA/cm²) and (2.17, 9.38 μA/cm²) at lower forward bias voltage V < 0.4V for S1 and S2 CZTS absorber based solar cells, respectively. For higher bias voltage, the observed change in slope in the lnI *vs* V characteristics is attributed to the enhanced carrier recombination because of increased minority carrier injection in the cell. Ideality factor greater than one substantiates the presence of unwanted recombination centers in the solar cell. We observed that S2 based solar cells exhibit lower recombination as compared to that of S1 absorber based solar cells. Thus, these results support that Cu poor and Zn rich configuration of CZTS (S2) is relatively advantageous to realize enhanced solar photovoltaic response as compared to Cu poor and Sn rich configuration (in present case S1 sample).

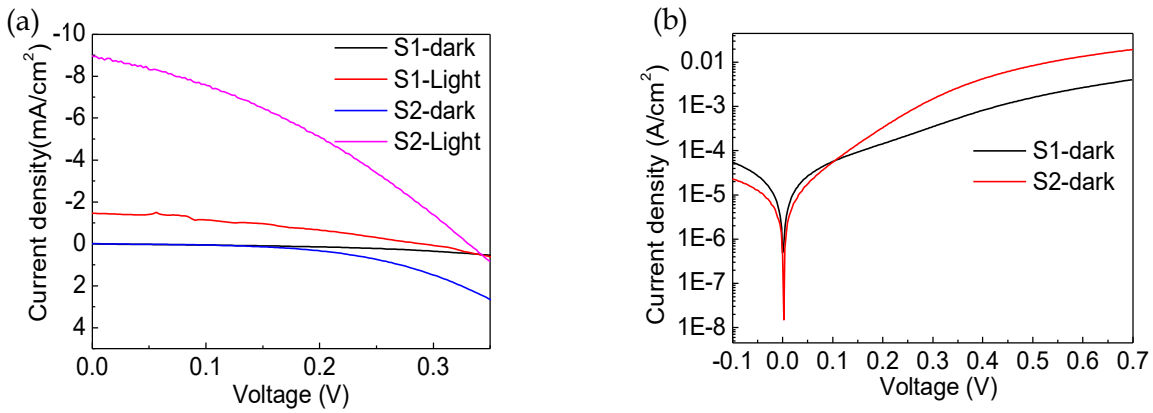

Figure 6.8 (a) Photovoltaic characteristics of CZTS solar cell with S1 and S2 absorber in dark and under illumination (b) Dark IV characteristics of S1 and S2 solar cell

Table 6.5 Photovoltaic device parameters, estimated from the measured photovoltaic response for devices based on S1 and S2 absorbers

Sample	Voc (V)	Jsc (mA/cm²)	FF (%)	Efficiency (%)	n	J_0 (μA/cm²)
S1	285	1.46	35	0.145	4.32	23.85
S2	331	9	35	1.0	2.17	9.38

6.9 Conclusion

A low cost sol-gel derived CZTS thin film synthesis process is used to achieve phase pure kesterite thin films. The low temperature processed sample S1 exhibits Sn rich stoichiometry, while s high temperature processed sample S2 exhibited substantial Sn loss and changes into slightly Zn rich and Cu, Sn poor stoichiometric conditions. Mössbauer measurements showed the presence of Sn at its preferred +IV oxidation states in both S1 and S2 samples and no significant peak is observed for Sn^{2+} state thereby reducing the possibility of presence of Sn_{Cu} donor defect. Large quadrupole splitting observed in S1 is possibly due to distortion at Sn site and the excess Sn composition also facilitate the presence of Sn at Zn site which is acting as a compensating donor defect to the available acceptor defects with low formation energy such as Cu_{Zn} and V_{Cu}. Further, the observed lower carrier concentration in S1 also validates this possibility. The high temperature processed S2 CZTS sample shows relatively better crystallization and thus, reduced lattice distortion as evidenced by the smaller QS splitting in Mössbauer spectra. The presence of less Sn in S2 reduces the possibility of Sn to occupy Cu or Zn site which is beneficial for the photovoltaic performance. This is supported by electrical and photovoltaic measurements, where solar cells based on S2 CZTS absorber showed enhanced photovoltaic response. The presented Mössbauer studies are very important to understand the available valance state of Sn in CZTS systems, which can be useful to properly investigate the defects and finally explaining the photovoltaic response.